Chemical Engineering Science 321 (2026) 122847

Contents lists available at ScienceDirect

Chemical Engineering Science

journal homepage: www.elsevier.com/locate/ces

A two-equation subgrid-scale model for Euler-Euler large eddy simulation of two-phase flows in bubble column reactors

Diego González [a,b], Anton Vernet [b], Bouchaib Gourich [c,d], Youssef Stiriba [b,*]

[a] Universidad Nacional de Asunción, Facultad de Ciencias Químicas, San Lorenzo, Paraguay
[b] Departament d'Enginyeria Mecanica, Universitat Rovira i Virgili, Av. Països Catalans 26, Tarragona, 43007, Catalonia, Spain
[c] Laboratory of Process and Environmental Engineering, Higher School of Technology, Hassan II University of Casablanca, Morocco
[d] International Water Research Institute (IWRI), Mohammed VI Polytechnic University, Ben Guerir, Morocco

ARTICLE INFO

Keywords:
Bubble column
Two-fluid model
Turbulence model
Large-eddy simulation
Two subgrid-scale model

ABSTRACT

This work presents a Euler-Euler Large Eddy Simulations (LES) two-fluid model for dispersed turbulent flows applied to simulate gas-liquid two-phase flows in bubble column reactors. The model is based on the one-equation model for the subgrid-scale (SGS) turbulent kinetic energy and develops a new transport equation for the subgrid-scale turbulent energy dissipation rate which avoids calculating the SGS turbulent length without referring to mesh size and offers the possibility to model more accurately physical phenomena at the SGS level. In this way, the amount of the SGS energy dissipation is employed to improve the modeling of the bubble induced turbulence (BIT). The BIT closure terms components are incorporated to the transport equations of the SGS turbulent kinetic energy and dissipation rate as a source term and the other component is added to the effective viscosity as a contribution of turbulence interaction. The new Euler-Euler two SGS model was implemented in the open-source OpenFOAM code and employed to simulate a two-phase bubble column reactor flow. The predicted liquid velocities and the turbulent kinetic energy are in good agreement with experimental data both in the core and the near-wall regions. The numerical simulations confirm that the energy spectra of the resolved liquid velocities in churn-turbulent regime follows the classical -5/3 law for low frequency regions and are close to -3 for high frequencies. To the best of our knowledge, this is the first use of a transport equation for SGS dissipation rate of turbulent kinetic energy in two-phase flows.

1. Introduction

Turbulent bubbly gas-liquid flows in multiphase reactors are important for many chemical, biochemical, electrochemical, and petrochemical industrial processes, and for environmental industries where bubble columns are employed. In bubble column reactors, the gas phase is dispersed in the form of tiny bubbles in a continuous liquid phase using a gas distributor. At high gas flow rates, the liquid phase flow becomes turbulent and, as the bubbles rise in the column, they induce also pseudo-turbulence in the liquid phase. This leads to bubble size distribution, which changes in space and time, bubble-bubble interactions, and complex flow structures. Furthermore, the presence of dispersed bubbles in a liquid turbulent flow affects the mechanism of turbulence production and dissipation, which becomes much more complex than single-phase mechanisms Kataoka et al. (1993), Dhotre et al. (2013), Joshi (2001), Liao et al. (2019). Indeed, turbulent bubbly flow is characterized by the development of distinct flow structures of wide range of scales. Turbulent scales may vary from those of the characteristic length of the mean flow to the bubble diameter and then to the Kolomogorov scale. For instance, the largest turbulence scales of motion are comparable in size to those of the mean flow and depend on the reactor geometry and flow conditions, whereas the smallest scales depend on the bubble dynamics and are proportional to the bubble size. Large-scale turbulent motions interact with the bubbles and thereby affect their motions, whereas small scales not only dissipate the kinetic energy but can generate energy to the largest scales and tend to be more isotropic as well Dhotre et al. (2013), Ma et al. (2015, 2016).

Several multiphase flow approaches have been proposed to correctly model the broad ranges of scales involved in such flows. These models lie between those representing the turbulence of the liquid phase or the mixture phases, such as the Reynold-Averaged Navier-Stokes (RANS) model with the ensemble averaged Euler-Euler approach for interpenetrating continua Mudde and Simonin (1999), Pfleger and Becker (2001), Tabib et al. (2008), to Euler-Euler large eddy simulation models which compute interaction of the large-scale motions with bubbles and model the less energetic smallest motions including the interaction of the

* Corresponding author.
E-mail address: youssef.stiriba@urv.cat (Y. Stiriba).

https://doi.org/10.1016/j.ces.2025.122847
Received 8 August 2025; Received in revised form 19 October 2025; Accepted 23 October 2025
Available online 8 November 2025

bubbles with the surrounding turbulence and represent them in terms of subgrid-scale closure models Deen et al. (2001), Ničeno et al. (2008), Dhotre et al. (2013), Ma et al. (2015, 2016), Goraki et al. (2020a). The Euler-Euler LES model predicts flows dominated by large coherent structures or eddies in bubble columns that carry most of the flow energy more accurately (typically 90 %) than traditional RANS models and represents more details of the flow structure Ma et al. (2015, 2016), Dhotre et al. (2008), Kouzbour et al. (2025). In addition, different Euler-Euler LES two-phase flow models have been proposed to simulate the unsteady behavior of bubbly flows in order to account for turbulent dispersion effects Deen et al. (2001), Ničeno et al. (2008). However, they cannot provide information on turbulent dissipation rates that are important for closure models such as bubble coalescence and breakup, as well as the mass transfer coefficient. The SGS turbulent dissipation is larger than the SGS turbulent kinetic energy and the molecular dissipation is very low, as pointed out by Li et al. Liu et al. (2020) in their review of the performance of LES in modeling bubbly flows. Besides, available bubble-induced source term models lie on the length and time scales, which are usually different from those characterizing single-phase flows. The filter width estimate may no longer be a good estimate for the characteristic SGS turbulence length when the filter cutoff is located at a wavenumber below the inertial range as pointed out by Chaouat and Schiestel (2005). Therefore, the characteristic scales calculations are accounted for by considering the turbulent dissipation rate.

In this work, we implement a two-equation LES model for subgrid-scale turbulent kinetic energy and turbulent kinetic energy dissipation rate used to model turbulence in two-phase flows. It is based on the single-phase self-adapting turbulence model developed by Perot and Gadebusch Perot and Gadebusch (2007) and may allow us to bridge the two-phase RANS and LES models. The model is compared with the SGS one-equation model introduced in Ničeno et al. (2008) by adding a new transport equation of the turbulent kinetic energy dissipation rate on the subgrid-scale. The interpenetrating phases are simulated with an Euler-Euler model, and the turbulence at the large scale is calculated with large-eddy simulation (LES). The main idea is to calculate the subgrid-scale turbulent dissipation energy that is often necessary to predict bubble-induced turbulence, some drag coefficient laws Brucato et al. (1998), the mass transfer coefficient, for instance the eddy cell model of Lamont and Scott (1970) which assumes that smaller eddies contribute more to the interface turbulence and to the mass transfer Wang et al. (2021), and in the population balance model rather than an estimation based on the resolved strain tensor in the liquid phase and the effective viscosity of the liquid.

In this paper, we start by introducing the general framework of the Euler-Euler LES model with all closure terms that comprise it in Section 2, a detailed description of the two-equation SGS model with a special emphasis on BIT is given in Sections 2.2 and 2.3. Then, the new two-fluid model is used to simulate gas-liquid flow in a bubble column reactor, and the predicted results and their comparison with the experimental data are presented in Section 3. Section 4 has a brief conclusion relevant to the performance of the two-equation LES model and some future applications and analysis.

2. Model formulation

The interdependency between the two-fluid model and the interfacial forces related to the bubbly flow in the liquid phase and the bubble interaction models is illustrated in Fig. 1. The two-fluid model calculates the velocity and volume fraction of both phases; these values are used to compute the interfacial forces and the bubble-induced turbulent viscosity (μ_{BIT}), which also depend on the constant bubble size considered in this work. The shear-induced turbulence terms S_k and S_ε depend on the drag force and a time scale that can employ the SGS parameters, which are detailed further in Section 3.3. Once the source terms for k_{SGS} and ε_{SGS} are calculated, both equations can be solved to calculate the subgrid-scale viscosity (μ_{SGS}) necessary to solve the two-fluid model equations for each phase, obtaining again the velocities and volume fractions. These complex interactions make modeling very difficult and highlight the importance of a two-equation SGS model, which motivates part of this work.

2.1. The LES model with Euler-Euler approach

The two-fluid model is based on phase filtering multiphase flow equations Dhotre et al. (2008), Lakehal (2018), where both phases, the continuous liquid phase and the dispersed gas phase, are modeled as two interpenetrating continua. The resulting interfacial interactions are the consequence of applying phase filtering as in volume averaging. In the present work, the flow is assumed to be adiabatic, without considering the interfacial mass transfer between the air and water phases.

In the LES filtering of the dispersed two-phase flow equations, both the contribution of the interfacial and turbulence scales are combined Lakehal (2018), Dhotre et al. (2008) and it is assumed that the filtered equations are used to resolve large-scale lengths while the effect of unresolved scales is modeled using a subgrid scale model.

The present formulation closely follows the procedure outlined by Weller (OpenCFD, Ltd., 2005), where the mass and momentum conservation equations for phase p are given by

$$\frac{\partial(\alpha_p\rho_p)}{\partial t} + \nabla\cdot(\alpha_p\rho_p\mathbf{U}_p) = 0, \quad p = L, G \tag{1}$$

$$\frac{\partial(\alpha_p\rho_p\mathbf{U}_p)}{\partial t} + \nabla\cdot(\alpha_p\rho_p\mathbf{U}_p\mathbf{U}_p) = -\alpha_p\nabla p_p + \alpha_p\rho_p\boldsymbol{g} - \nabla\cdot\left(\alpha_p\tau_p^{\text{eff}}\right) + \boldsymbol{M}_p \tag{2}$$

Here α_p is the volume fraction of each phase, $\mathbf{U}_p$ is the phase resolved velocity, and τ_p^{eff} represents the effective stress tensor which is usually decomposed into a mean viscous stress and turbulent stress tensor for phase p as

$$\tau_p^{\text{eff}} = \mu_p^{\text{eff}}\left(\nabla\mathbf{U}_p + (\nabla\mathbf{U}_p)^T - \frac{2}{3}(\nabla\mathbf{U}_p)\mathbf{I}\right) + \frac{2}{3}k_p\mathbf{I} \tag{3}$$

where k_p is the turbulent kinetic energy of phase p, $\mathbf{I}$ is the identity tensor, and μ_p^{eff} is the effective viscosity of phase p. The effective viscosity of the liquid phase is obtained through the contribution of the molecular viscosity, the shear-induced turbulent viscosity, and the bubble-induced turbulent viscosity that reflects the interaction between the phases

$$\mu_p^{\text{eff}} = \mu_{p,L} + \mu_{p,SGS} + \mu_{p,BIT} \tag{4}$$

The SGS eddy shear-induced viscosity may be scaled according to the Smagorinsky model Zhang et al. (2006)

$$\mu_{p,SGS} = (C_S\Delta)^2|S| \tag{5}$$

where C_S is a model constant, S is the characteristic filtered rate of the strain and $\Delta = Vol^{1/3}$ is the filtered width calculated from Vol the volume of the computational cell. Dhotre et al. 2008 Dhotre et al. (2008) employed the dynamic model of Germano Germano et al. (1991) to have estimates of C_S values and the model of Sato Sato and Sekoguchi (1975) for $\mu_{p,BIT}$. Niceno et al. 2008 Ničeno et al. (2008) applied the one-equation LES model to two-phase flows by solving a transport equation for the SGS kinetic turbulent energy and introduced an additional source term to account for the effect of the other phase.

In Eq. (2), $\mathbf{M}_p$ represents the interphase momentum exchange between the bubbles and the liquid phase due to various interphase forces. The interfacial forces are driven by the momentum transfer from the bubble flow and can be decomposed into several contributions as follows

$$\mathbf{M}_p = \mathbf{M}_p^D + \mathbf{M}_p^L + \mathbf{M}_p^{VM} + \mathbf{M}_p^{TD} \tag{6}$$

Here the forces on the right-hand side of equality, for the liquid phase, are

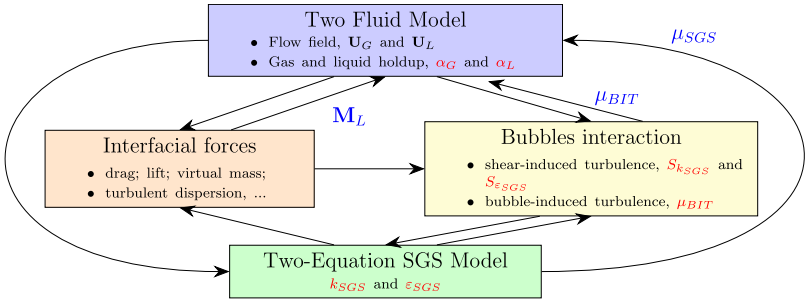

Fig. 1. Schematic of the inter-dependency of the two-fluid model, interfacial force, the bubbles interaction and the two equatons SGS model.

- the drag force, $\mathbf{M}_L^D$, which represents a resistance opposed to the particles due to the presence of the continuous phase, and can be modeled as (Clift et al., 1978)

$$\mathbf{M}_L^D = \frac{3}{4}\frac{C_D \rho_L \alpha_G}{d_B}|\mathbf{U}_G - \mathbf{U}_L|(\mathbf{U}_G - \mathbf{U}_L) \tag{7}$$

where the drag law coefficient C_D is a model coefficient, and it is calculated using the Ishii and Zuber (Ishii and Zuber, 1979) model as follows

$$C_D = \max\left[C_{D,\text{sphere}}; \min\left(C_{D,\text{ellipse}}; C_{D,\text{cap}}\right)\right] \tag{8}$$

where

$$C_{D,\text{sphere}} = \begin{cases} \frac{24}{Re_m}\left[1 + 0.10\left(Re_m\right)^{0.75}\right] & Re_m < 1000 \\ 0.44 & Re_m \geq 1000 \end{cases} \tag{9}$$

$$C_{D,\text{ellipse}} = \frac{2}{3} Eo\, f(\alpha_G) \tag{10}$$

$$C_{D,\text{cap}} = \frac{8}{3}\left(1 - \alpha_G\right)^2 \tag{11}$$

Here Eo is the dimensionless Eötvös number, which represents the relation between the gravitational and surface tension (σ) forces, and Re_m is the mixture Reynolds number, each one defined as:

$$Eo = \frac{(\rho_L - \rho_G) g\, d_B^2}{\sigma} \tag{12}$$

$$Re_m = \frac{\rho_L\, d_B\, |\mathbf{U}_G - \mathbf{U}_L|}{\mu_m} \tag{13}$$

The mixture viscosity μ_m, and the correction function $f(\alpha_G)$ in $C_{D,ellipse}$ are also detailed in the work (Ishii and Zuber, 1979).

- the lift force, $\mathbf{M}_L^L$, considered a perpendicular force to the direction of the bubble motion to reproduce its radial dispersion, and it is modeled according to (Auton, 1987; Drew and Lahey, 1987):

$$\mathbf{M}_L^L = \alpha_G \rho_L C_L (\mathbf{U}_G - \mathbf{U}_L) \times \nabla \times \mathbf{U}_L \tag{14}$$

where C_L is a model coefficient, with constant value of 0.5.

- the added mass force, $\mathbf{M}_L^{VM}$, accelerates the fluid that surround the particle, and often it is called virtual mass force, and can be modelled as in (Auton, 1987; Drew and Lahey, 1987):

$$\mathbf{M}_L^{VM} = \alpha_G \rho_L C_{VM}\left(\frac{D\mathbf{U}_G}{Dt} - \frac{D\mathbf{U}_L}{Dt}\right) \tag{15}$$

where C_{VM} is a model coefficient, with a constant value of 0.5.

- the turbulent dispersion force, $\mathbf{M}_L^{TD}$, represents the turbulent dispersion influence of the turbulent eddies on the filtering of the drag force and can be modeled according to Lopez de Bertodano (Lopez de Bertodano et al., 1994) as:

$$\mathbf{M}_L^{TD} = C_{TD}\, \rho_L\, k_{SGS} \nabla \alpha_G \tag{16}$$

where C_{TD} is the turbulent dispersion coefficient.

There are many models for each of these interfacial forces, and their descriptions depend on their applicability, flow regime, reactor geometry, and operating conditions, as discussed by Joshi (2001), Tabib et al. (2008), Vial and Stiriba (2013), Goraki et al. (2020a), Kouzbour et al. (2021). There is still no complete agreement on the closures or the combination to be used at best. For example, the inclusion of the turbulent dispersed force did not show any improvement for the present test case, since the bubble size employed is relatively larger as the filter width and the SGS motion. Compared with our previous work Goraki et al. (2020a,b), this interfacial force works quite well for bubbly flow in a cylindrical pilot-scale bubble column, where a small bubbles of moves near close to the wall reactor. For the lift force, we used the Tomiyama model Tomiyama et al. (2002), but no noticeable improvements in the results were observed, which led us to conclude that this interfacial force plays a minor role in our test cases. For spherical bubbles with small constant diameter of 4 mm, a constant lift coefficient of 0.5 can be used, since the lift force is perpendicular to the movement of the fluid that tends to push the bubbles outward towards the wall column ($C_L > 0$). The lift coefficient of Tomiyama is approximately $C_L \approx 0.29$, consequently, the dispersion of the bubble plume is reduced compared to lift coefficient with $C_L = 0.5$, which leads to a relatively steep vertical velocity profile. Furthermore, steady simulations of a bubble column reactor Vial and Stiriba (2013) show that the lift force was overshadowed by the turbulent dispersion force which better predicted the radial dispersion of the gas phase along the axial direction of a cylindrical bubble column and the experimental gas holdup at the center of the column using a single orifice nozzle. The virtual mass, which is also considered in this work, does not have an impact on the results either, similar to the lift force effect mentioned. No swarm correction is considered for the simulations since the gas hold up is lower according to Simonnet et al. Simonnet et al. (2007) and Behzadi et al. Behzadi et al. (2004) swarm factor correlations.

2.2. The two-equation model

Turbulent models that aim to solve multiphase flows, such as large eddy simulations, require modeling turbulent dissipation. The two-phase flow one-equation model of Ničeno et al. (2008) avoids the necessity of resolving down to Kolmogorov scales and employs the relation

$$\varepsilon_{SGS} = C_\varepsilon \frac{k_{SGS}^{3/2}}{l} \tag{17}$$

to estimate the turbulent dissipation rate of the unresolved scales, where k_{SGS} is the kinetic energy, l is an integral scale equal to the grid filter and C_ε a dimensionless coefficient that is constant at a Reynolds number large enough or computed dynamically.

The present two-equation model solves two transport equations for the subgrid-scale kinetic energy, k_{SGS}, and the dissipation rate ε_{SGS}

$$\frac{\partial k_{SGS}}{\partial t} + \nabla \cdot \left(k_{SGS}\mathbf{U}_p\right) = \nabla \cdot \left[(\nu_p + \nu_{SGS})\nabla k_{SGS}\right] + \alpha P_k - \varepsilon_{SGS} \tag{18}$$

Latin Letters

$\mathbf{M}_p$	inter-phase momentum exchange between phase p and the other phase
$\mathbf{U}'_p$	phase fluctuating velocity (m/s)
$\mathbf{U}_p$	phase resolved velocity (m/s)
$\mathbf{M}^D$	drag force (N/m^2)
$\mathbf{M}^L$	lift force (N/m^2)
$\mathbf{M}^{VM}$	virtual mass force (N/m^2)
C_D	drag force coefficient
C_L	lift force coefficient
C_S	Smaroginsky constant
C_{VM}	virtual mass force coefficient
d_B	gas bubble diameter (m)
Eo	Eotvos number
k_p	turbulent kinetic energy of phase p(m^2/s^2)
k_{SGS}	SGS turbulent kinetic energy (m^2/s^2)
Re_M	mixture Reynolds number

Greek Letters

α_l, α_g	liquid, gas volume fraction
Δ	filter width (m)
ε_{SGS}	SGS turbulent dissipation rate (m^2/s^3)
$\mu_{p,BIT}$	bubble induced viscosity (m^2/s)
$\mu_{p,L}$	molecular viscosity (m^2/s)
$\mu_{p,SGS}$	SGS eddy shear induced turbulent viscosity (m^2/s)
ν_p^{eff}	effective viscosity of phase p (m^2/s^2)
τ_{time}	time scale for BIT (s)
ε	resolved dissipation of turbulent kinetic energy (m^2/s^3)

Subscripts

p	phase ($p = G$ gas phase; $p = L$, liquid phase

$$\frac{\partial \varepsilon_{SGS}}{\partial t} + \nabla \cdot \left(\varepsilon_{SGS}\mathbf{U}_p\right) = \nabla \cdot \left[(\nu_p + \nu_{SGS})\nabla \varepsilon_{SGS}\right] + \frac{\varepsilon_{SGS}}{k_{SGS}} \left(C_{\varepsilon 1} P_k - C_{\varepsilon 2}\varepsilon_{SGS}\right) \tag{19}$$

where k_{SGS} and ε_{SGS} are given without the lower index L for simplicity. The shear-induced production term is defined as

$$P_k = \nu_{SGS}\,\mathbf{S} : \mathbf{S}, \qquad \mathbf{S} = \text{sym}\left(\nabla \mathbf{U}_p\right) \tag{20}$$

The model constants $C_{\varepsilon 1}$ and $C_{\varepsilon 2}$ are equal to the standard $k-\varepsilon$ constants, and α is an energy transfer parameter, as suggested in Perot and Gadebusch (2007). The present model based on two transport equations at the subgrid-scale may allow us to incorporate more accurately the turbulent processes of production, transfer, and dissipation. Furthermore, a successful LES must have a filter width Δ in the intertial range and it will not be a good estimate for the Euler-Euler-LES model where the bubble size d_B is larger than Δ, Chaouat and Schiestel (2005). According to Dhotre et al. 2008 Dhotre et al. (2008), such large bubbles would induce large-scale motion and may deteriorate the accuracy of the resolved large-scales. The best for the model is to have a mesh where bubbles-induced scales fall in the SGS. Therefore, the present model avoids calculating the SGS turbulent length using the calculated dissipation ε_{SGS}.

The subgrid-scale viscosity is calculated as in the same way as for a single-phase flow Perot and Gadebusch (2007)

$$\nu_{SGS} = C_\mu \frac{k_{SGS}^2}{\varepsilon_{SGS}} \left(\frac{k_{SGS}}{k_{SGS} + k_r}\right) \tag{21}$$

where $C_\mu = 0.18$ and $k_r = \frac{1}{2}(\mathbf{U}'_p)^2$ is the resolved turbulent kinetic energy, and ε_{SGS} is the modelled dissipation of the resolved dissipation of turbulent kinetic energy $\varepsilon = \nu(\mathbf{U}'_p\mathbf{U}'_p)$. If the quantity $\frac{k_{SGS}}{k_{SGS}+k_r} \to 1$ the model switches to RANS eddy viscosity and if it is small the LES eddy visocity scales with the mesh size as the turbulent length scale Perot and Gadebusch (2007).

To account for the back scatter energy effects from the modeled turbulence to the resolved turbulence, we employ the same energy transfer energy variable α, developed and tuned by Perot and Gadebusch (2007), both in the stress tensor term and the production term in the subgrid-scale turbulent kinetic energy. It tends to deliver energy from the model to the resolved flow at the same scale and enhances the turbulent intensity induced by the bubbles.

The new Euler-Euler two subgrid-scale model is implemented in the OpenFOAM open source computational fluid dynamics (CFD) package library Weller et al. (1998) by adding constants and functionality from the existing two-phase `NicenoKEqn` turbulence model, which solves the transport equation of the turbulent kinetic energy modeled, to the new two-equation SGS model. Time discretization was performed using a first-order bounded implicit Euler scheme and the spatial discretization with Gauss finite volume method with central differencing for interpolation. Gradients are approximated with a linear interpolation. The PIMPLE algorithm is employed to solve the pressure-velocity coupling, where the discretized pressure equation is solved with the geometric algebraic multigrid method. We refer the reader to the work of Rusche (2002) for a more detailed discussion of those steps.

2.3. The bubble-induced turbulence

Bubble-induced turbulence (BIT) is one of the most relevant closures for multiphase flow models, and numerous models have been developed to incorporate bubble effects properly. It is also possible to account for their effects through an additional viscosity, μ_{BIT}, for the turbulence interaction applied to the continuous phase, as suggested by Sato and Sekoguchi Sato and Sekoguchi (1975), or using an additional source term, P_{BIT}, in the $k-\varepsilon$ transport equation Pfleger and Becker (2001), Troshko and Hassan (2001), Rzehak and Krepper (2013b). In fact, the additional production of turbulent kinetic energy is due to the inter-phase drag force, $S_{k_{SGS}}$, and the destruction of the BIT for the turbulence dissipation is assumed to be proportional to the production rate divided by a time scale τ_{time} in Eq. (19)

$$S_{k_{SGS}} = M_L^D\left(\mathbf{U}_G - \mathbf{U}_L\right) \tag{22}$$

$$S_{\varepsilon_{SGS}} = C_{\varepsilon b}\frac{S_{k_{SGS}}}{\tau_{\text{time}}} \tag{23}$$

In the present model, both approaches were analyzed and three time scales were used. The detailed type of time scale and the value of the parameter corresponding to $C_{\varepsilon b}$ are presented in Table 1.

The time scale represents the lifetime of turbulent eddy before it breaks up into smaller structures and is defined as the ratio of the character length scale to the character velocity scale. It may be related to bubble diameter, turbulent kinetic energy, turbulent dissipation rate, and two-phase slip velocity. For instance, the time scale τ_1 is related to the bubble size and the relative velocity and independent from turbulence parameters that is more suitable for BIT modeling than the eddy size in the wake behind the bubble, Liao et al. (2019). The time scale model τ_2 employs the bubble diameter for the characteristic length scale and the SGS turbulent kinetic energy. The time scale τ_3 depends both on the modeled SGS kinetic energy and the dissipation rate. A detailed comparison between those characteristic scales is presented in Subsection 3.2.

Therefore, the characteristic scales calculations are accounted for by considering the turbulent dissipation rate, that is necessary to calculate the bubble-induced turbulence, some drag coefficient laws like those developed by Brucato et al. (1985) Brucato et al. (1998), and in the population balance model kernels rather than an estimation based on the resolved strain tensor in the liquid phase and the effective viscosity of the liquid. To the best of our knowledge, this is the first use of a transport equation for SGS dissipation rate of turbulent kinetic energy in two-phase flows. Furthermore, Han et al. Han et al. (2016) showed

Table 1
Time scales factor used and $C_{\epsilon b}$ values in ϵ_{SGS} source term.

Length scale l	Velocity scale u	Time scale τ_{time}	$C_{\epsilon b}$	References
d_B	$\lvert\mathbf{U}_G - \mathbf{U}_L\rvert$	$\tau_1 = d_B/\lvert\mathbf{U}_G - \mathbf{U}_L\rvert$	0.45	Bubble time scale, Troshko and Hassan (2001)
d_B	$\sqrt{k_{SGS}}$	$\tau_2 = d_B/\sqrt{k_{SGS}}$	2.0	Mixed time scale, Rzehak and Krepper (2013a)
$k_{SGS}^{3/2}/\epsilon_{SGS}$	ϵ_{SGS}	$\tau_3 = k_{SGS}/\epsilon_{SGS}$	1.44	Turbulent time scale, Pfleger and Becker (2001)

Table 2
Simulation cases.

BIT mechanism on liquid phase	Time scale factor for ϵ_{SGS} source term
Only BIT viscosity	BTS MTS TTS
Only source terms in k_{SGS} and ϵ_{SGS} conservation equations	BTS MTS TTS
BIT viscosity and source terms in k_{SGS} and ϵ_{SGS} conservation equations	BTS MTS TTS

BTS: bubble time scale, MTS: mixed time scale, TTS: turbulent time scale

that the estimation of the mass transfer coefficient needs, the dissipation range which contributes to the main part of the mass transfer rate and requires an accurate estimate of ϵ_{SGS}.

3. Results and discussion

To test our formulation and validate the implementation of the two-equation LES turbulence model in the open source CFD code OpenFOAM, the experimental data of the bubble column from (Deen et al., 2001) is used. The test case has a simple geometry and initial and boundary conditions. Other authors have used it to test their turbulence models for Euler-Euler LES of dispersed bubbly flows such as the zero-equation Smagorinsky and the one-equation SGS model Zhang et al. (2006), Liu and Li (2018), Masood and Delgado (2014), Ničeno et al. (2008). We start by validating the model with different computational meshes in terms of gas volume fraction, axial gas and liquid velocities, and turbulence parameters. Then, we analyze the capability of the model in capturing the fluctuating turbulence of the instantaneous flow behavior and the performance of the model with and without additional BIT terms. The power spectral density for the fluctuating liquid velocity is also discussed.

The bubble column reactor of Deen et al. 2000 (Deen et al., 2001) has dimensions of width and depth of 0.15 m, and height of 0.5 m. The reactor operates in batch mode with 0.45 m of initial static height of the liquid, and the sparger is a square of size 0.03 m located in the center of the column. The continuous and dispersed phases are water and air, respectively, at room temperature and atmospheric pressure. A constant superficial gas velocity of 0.0049 m/s is used for the simulation, with a nearly homogeneous bubble size distribution of constant diameter equal to 4 mm obtained from experimental measurements (Deen et al., 2001). This justifies the bubble size used in the present two-fluid model approach. Two grid refinements are employed, $15 \times 50 \times 15$ and $30 \times 100 \times 30$, which correspond to the ratios of $\Delta/d_B = 2.5$ and $\Delta/d_B = 1.25$, respectively. The time step is 0.005 s for the coarse grid, and 0.001 s for the refined one, the total simulation time is 200 s, and the averaging quantities were taken between 25 and 200 s.

Development of BIT as source term or additional viscosity, either for RANS models or LES zero- and one-equation models, was analyzed and reviewed by several authors but no generally statisfactory model has been developed so far and there is no direct relationship between a specific condition or application and the way to include the BIT effects in the continuous phase, see Ničeno et al. (2008), Rzehak and Krepper (2013b), Goraki et al. (2020a). In order to explore the two equation turbulence model performance, and evaluate the hydrodynamic of the flow, the simulations have been carried out by considering the BIT effect through the source terms of k_{SGS} and ϵ_{SGS}. the bubble induced viscosity model, and a combination of both effects. The three time scale constants for the source term ϵ_{SGS} presented in Table 1 are used in the simulations. The list of simulation cases is given in Table 2.

3.1. Grid comparison results

A comparison of the mean axial velocity profiles of the gas and liquid and the mean resolved turbulent kinetic energy is made by experimental data from (Deen et al., 2001) for the two grid sizes considered. All profiles are evaluated at height $y = 0.25$ m in the center of the column. The numerical study of (Milelli, 2002) recommended a ratio between the bubble diameter and the grid size of $\Delta/d_B \geq 1.5$. In our case, the coarse grid satisfied this condition and the fine one did not. Fig. 2 shows the instantaneous and mean axial water velocities, calculated between 25 and 200 s, for the case with only source terms for the bubble-induced turbulence effect, and the turbulence time scale. The flow was simulated for 200 s. It can be seen that the mean values tend to be uniform, especially between 150 and 200 s, ensuring that before we start to collect statistics the solution has been reasonably statistically stable.

In Fig. 3(a) and (b), the mean axial velocities of gas and liquid for the two grids are compared with experimental data. For all cases, the results with the coarse grid overestimated the values of both velocities in the center of the column. Also, unlike what is expected, both velocities are well approximated to the experimental values near-wall regions. Even though better results are obtained with the finer grid, it is worth mentioning that this grid does not satisfy the grid/bubble diameter ratio condition, although the difference is small.

In Fig. 3(c), the mean resolved turbulent kinetic energy is compared between the two grids and the experimental values. As in the results of mean velocities, the values obtained with the coarse mesh are overestimated in the center of the column; besides, the experimental values present a decay in the center of the column, which is not captured well for the coarse grid; however, a good approximation near wall regions is obtained for all cases. For the finer grid, in all cases the values are lower in the center of the column, getting closer to the experimental values; it is important to notice that only in the case with mixed time scale and

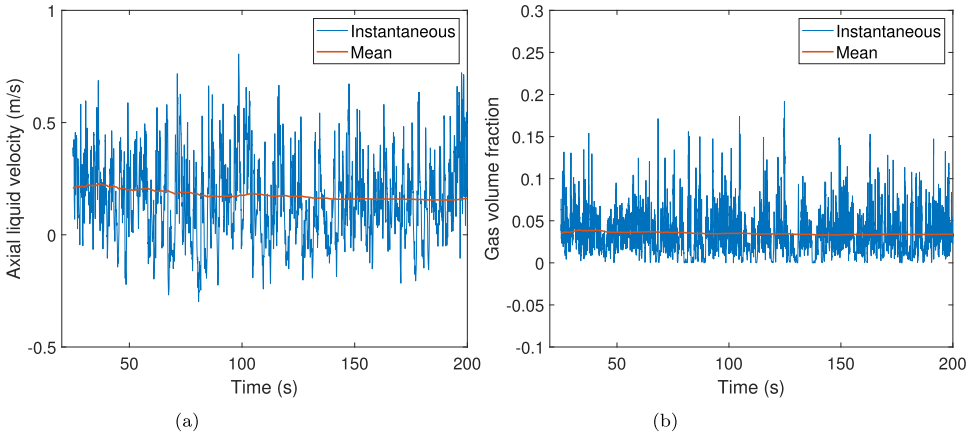

Fig. 2. Time series and mean values for liquid velocity (a) and gas volume fraction (b) in point $x = y = z = 0.25$ m.

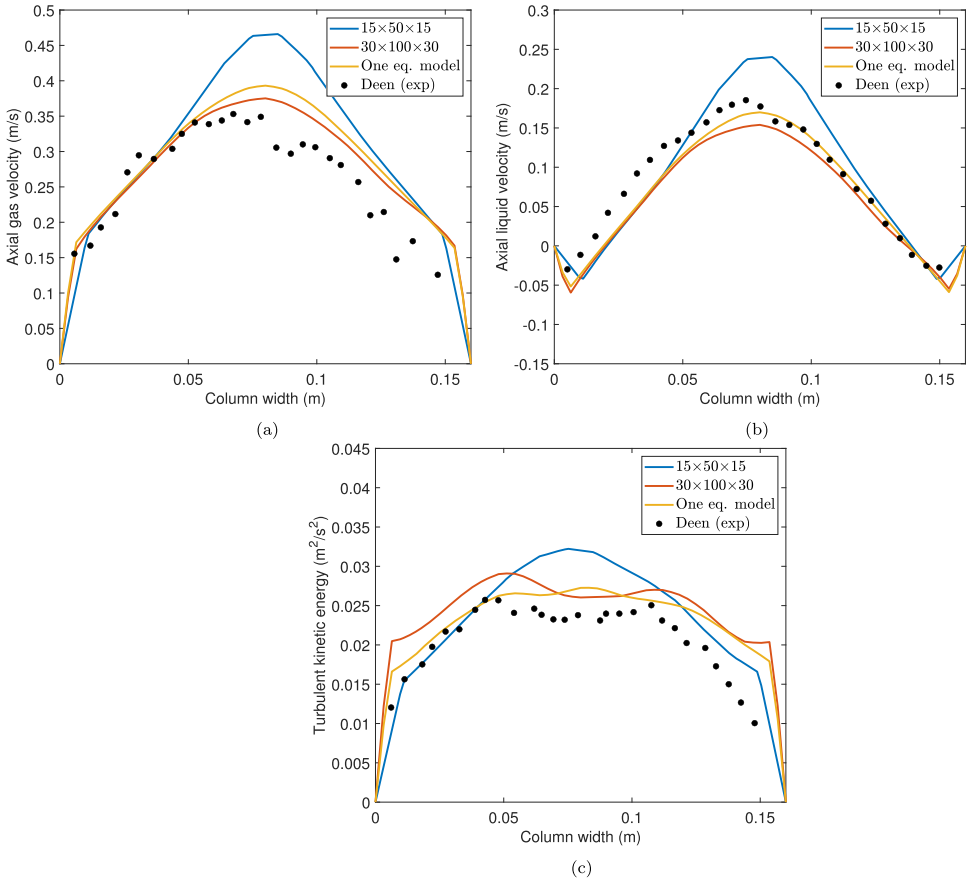

Fig. 3. Mean velocities and resolved turbulent kinetic energy for two grids.

turbulence time scale for the source term, the profile behavior is well captured; for instance, the lower values are in the center and peak values at x values of 0.04 and 0.11 m, although the values of the resolved turbulent kinetic energy are slightly above the experimental data.

The two-equation model is also tested against the one-equation model of Niceno et al. 2008 Ničeno et al. (2008) using the finer mesh in Fig. 3. Although both models show good agreement for the axial gas and liquid velocities, the present model reproduces well the double-peaked shape profile, observed in experimental measurements, of the resolved kinetic energy in the core center of the column and slightly overpredicts the profile close to the left wall.

3.2. *Performance of the two-equation subgrid-scale model*

In this section, the ability of the two-equation LES turbulence model is tested to capture the transient characteristics of instantaneous flow in a bubble column. Some of the main features are the spiral movement from the bottom to the top of the bubble plume, the recirculating zones in the near-wall regions, and the presence of multiple eddies of different sizes, which vary over time. These features are obtained through observations and experimental measurements, as in the works of (Chen et al., 1994; Pfleger et al., 1999; Degaleesan et al., 2001), and numerical simulations such as (Joshi, 2001; Goraki et al., 2020a).

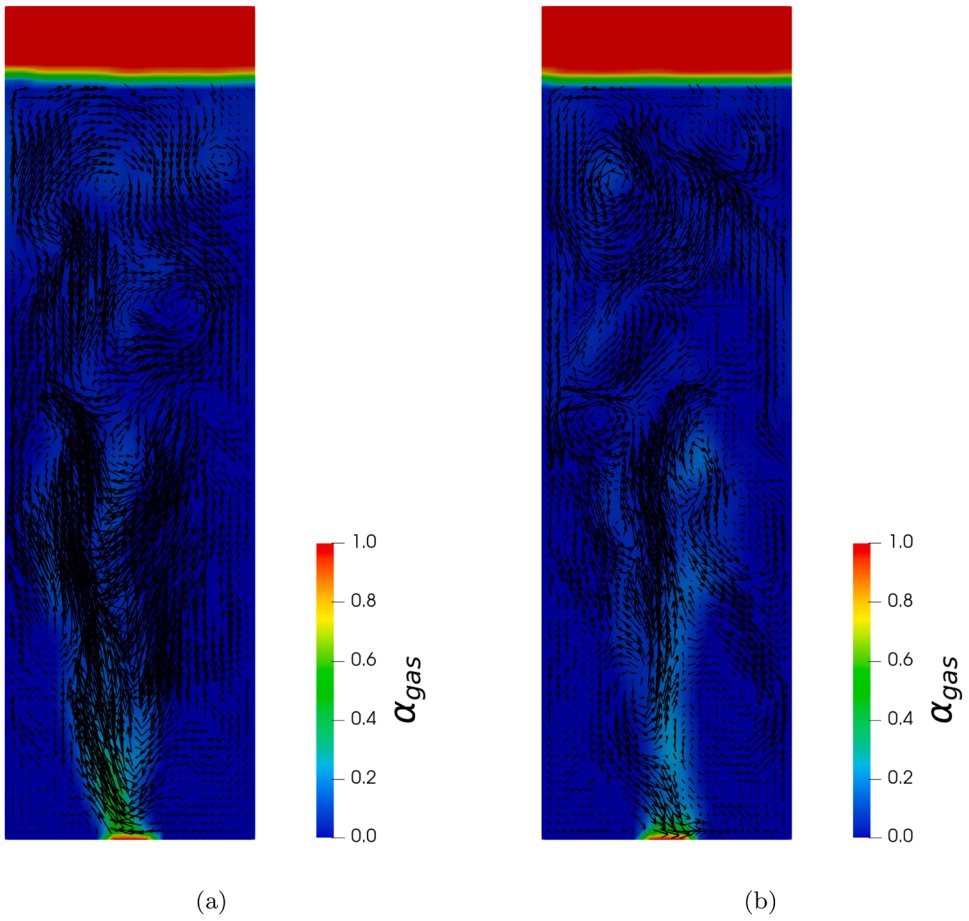

Fig. 4. Fluctuating liquid vector velocity and contour gas volume fraction for (a) Time 50 s and (b) Time 150 s.

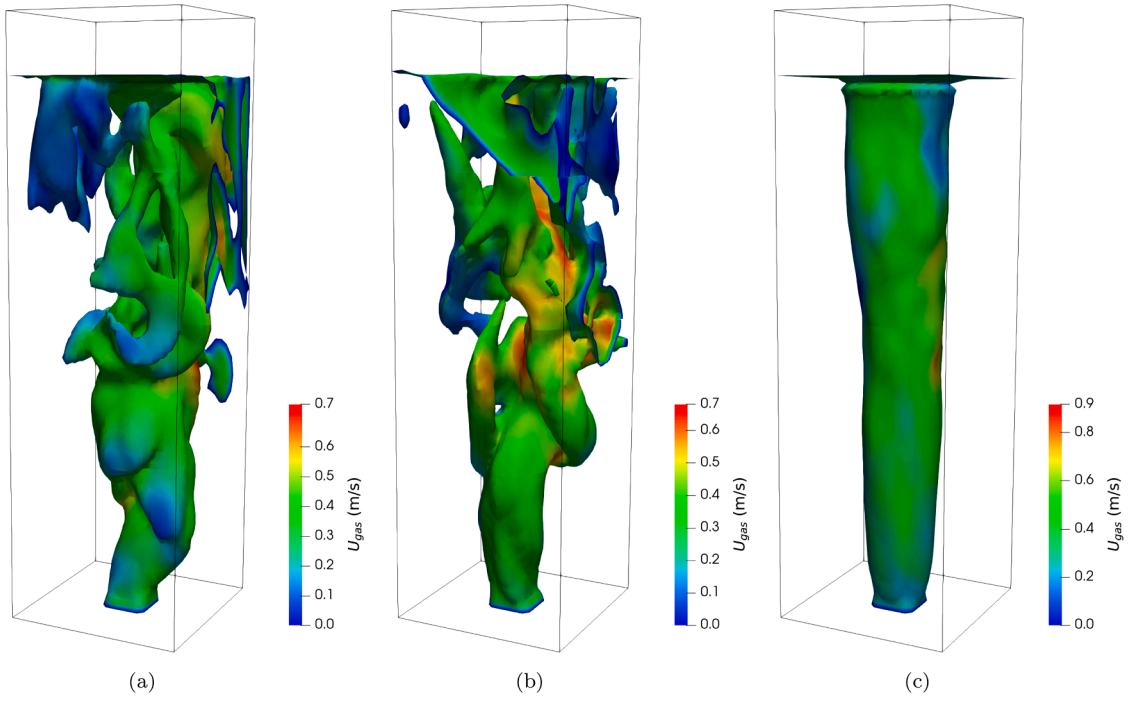

Fig. 5. Instantaneous and mean gas volume fraction isosurfaces of $\alpha_g = 0.025$, coloured with instantaneous gas velocity magnitude (a) Time 100 s (b) Time 200 s and c) Mean between 25–200 s.

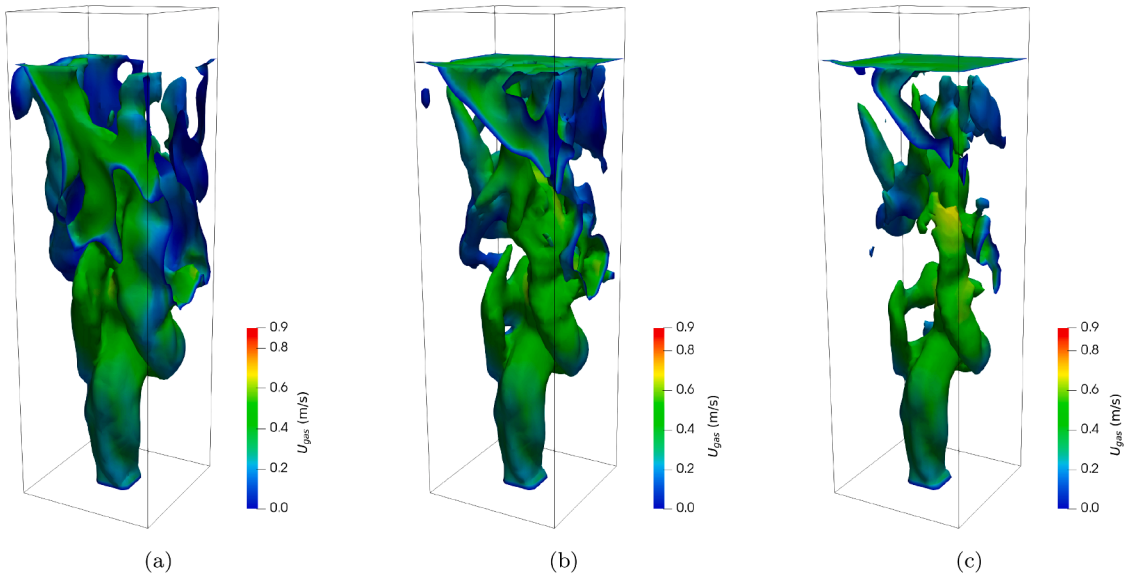

Fig. 6. Instantaneous gas volume fraction isosurfaces at time 200 s, coloured with instantaneous gas velocity magnitude (a) $\alpha_g = 0.01$ (b) $\alpha_g = 0.025$ and c) $\alpha_g = 0.04$.

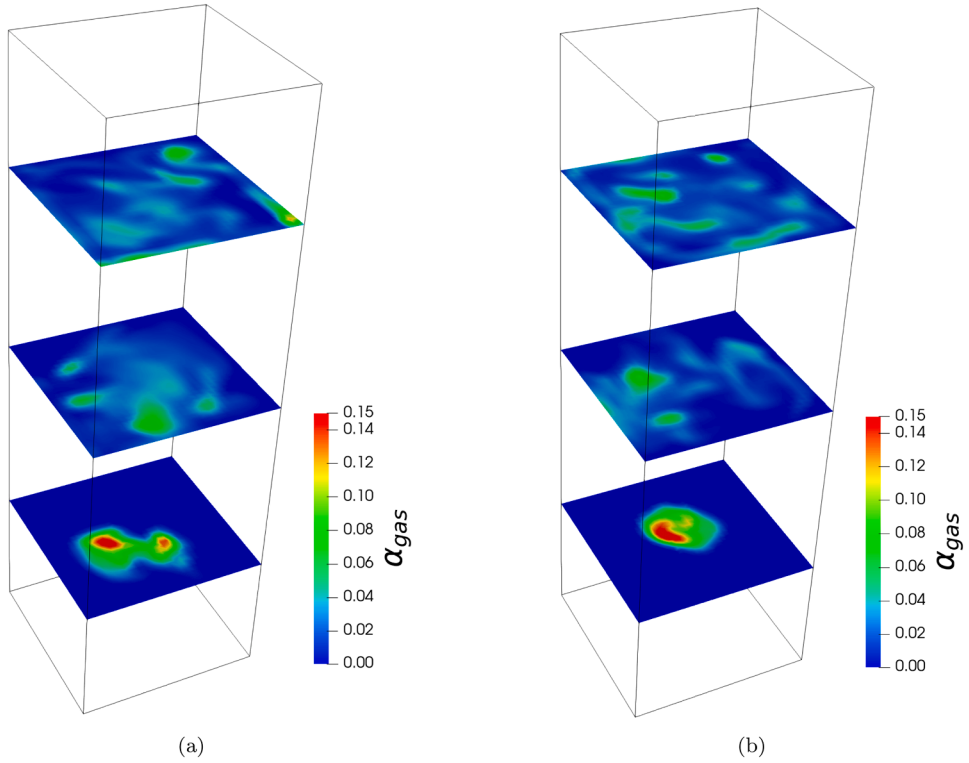

Fig. 7. Snapshots of gas volume fraction for (a) Time 100 s and (b) Time 200 s, in $y = 0.1, 0.2, 0.3, 0.4$ m.

In Fig. 4, the snapshots of the vector flow field of the instantaneous fluctuating liquid velocity and the contour of the gas volume fraction are displayed at two different times, 50 a and 150 s. The velocity vectors show an upward main movement in the center of the column, and the descending flow is observed near both wall regions. For each time, the recirculation zone occurs near only one of the walls, indicating the transient nature of the flow and it's wavy movement. Alongside the central plume, multiple eddies with small and large sizes are encountered, which change in position over time, showing the anisotropic and transient behavior of turbulence.

In Figs. 5 and 6, different isosurfaces of the gas volume fraction colored with the magnitude of the gas velocity are shown, and in Fig. 7 snapshots of the gas volume fraction $\alpha_G = 0.025$ colored also by the magnitude of the gas velocity field in different cross sections of the column are shown, at different times. The gas isosurfaces change in time and are asymmetric within the bubble plume with a more pronounced lateral spreading from the height center to the free surface level. The inclination toward different sides of the walls is also appreciated, emphasizing the gas flow in a vortical-spiral pattern alongside the column. Initially, bubbles rise uniformly as a group and, as they increase, they will break

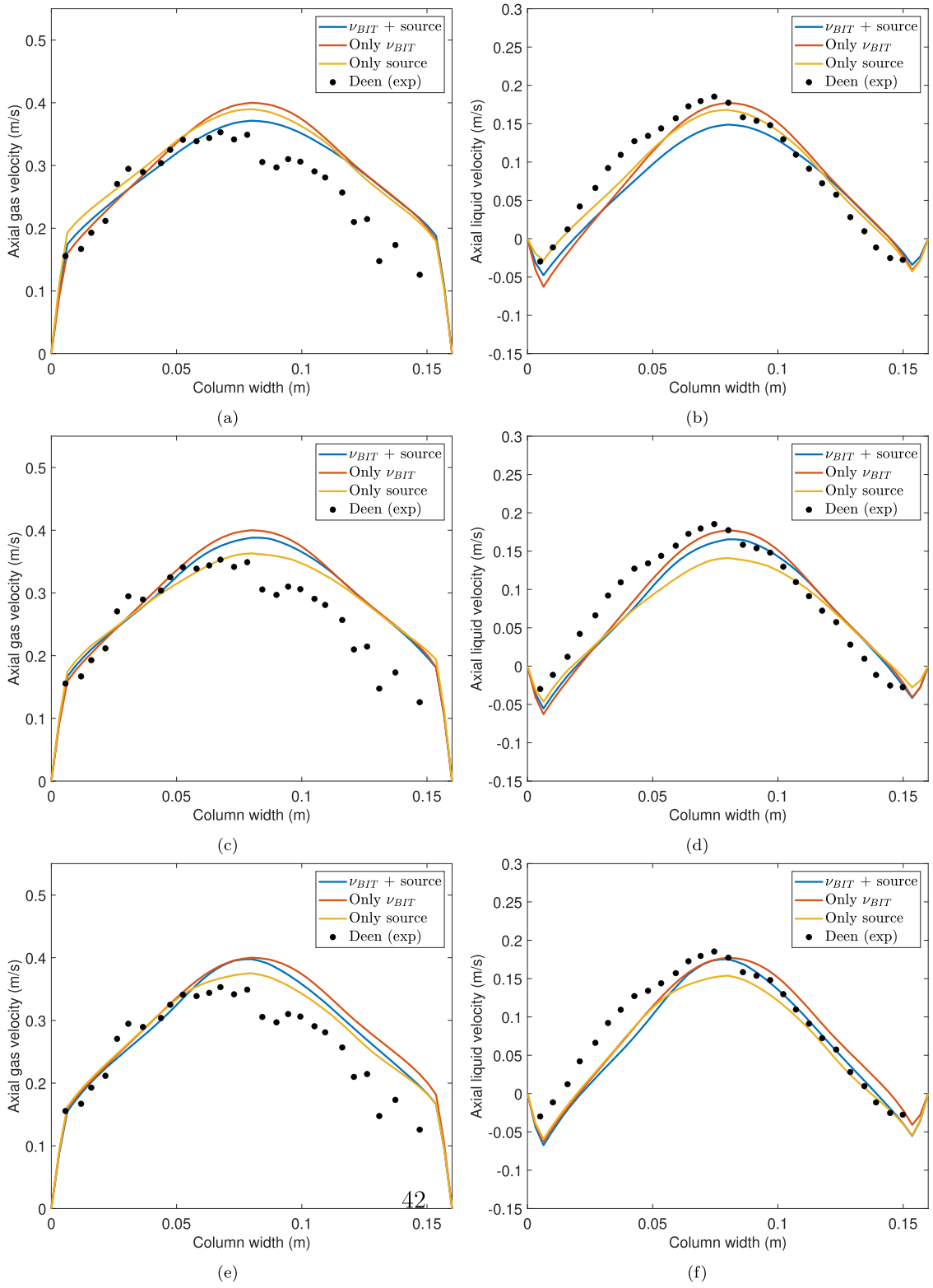

Fig. 8. Mean velocities for both phases using: BTS in ε_{SGS} source term (top), MTS in ε_{SGS} source term (middle), and TTS in ε_{SGS} source term (bottom).

and disperse because of the effect of liquid turbulence. The low values of the gas volume fraction showed in Fig. 6 are obtained because the superficial gas velocity at the inlet is not high, as it only enters and spreads along the central part of the column. Contour plots of gas volume fraction also show the gas distribution in different sections of the column, indicating the wavy motion of the bubble plume and a dispersed gas phase toward the walls.

Considering that the details of the transient flow encountered in the simulation results are in agreement with experimental measurements and other simulations, the two-equation LES model presented in this

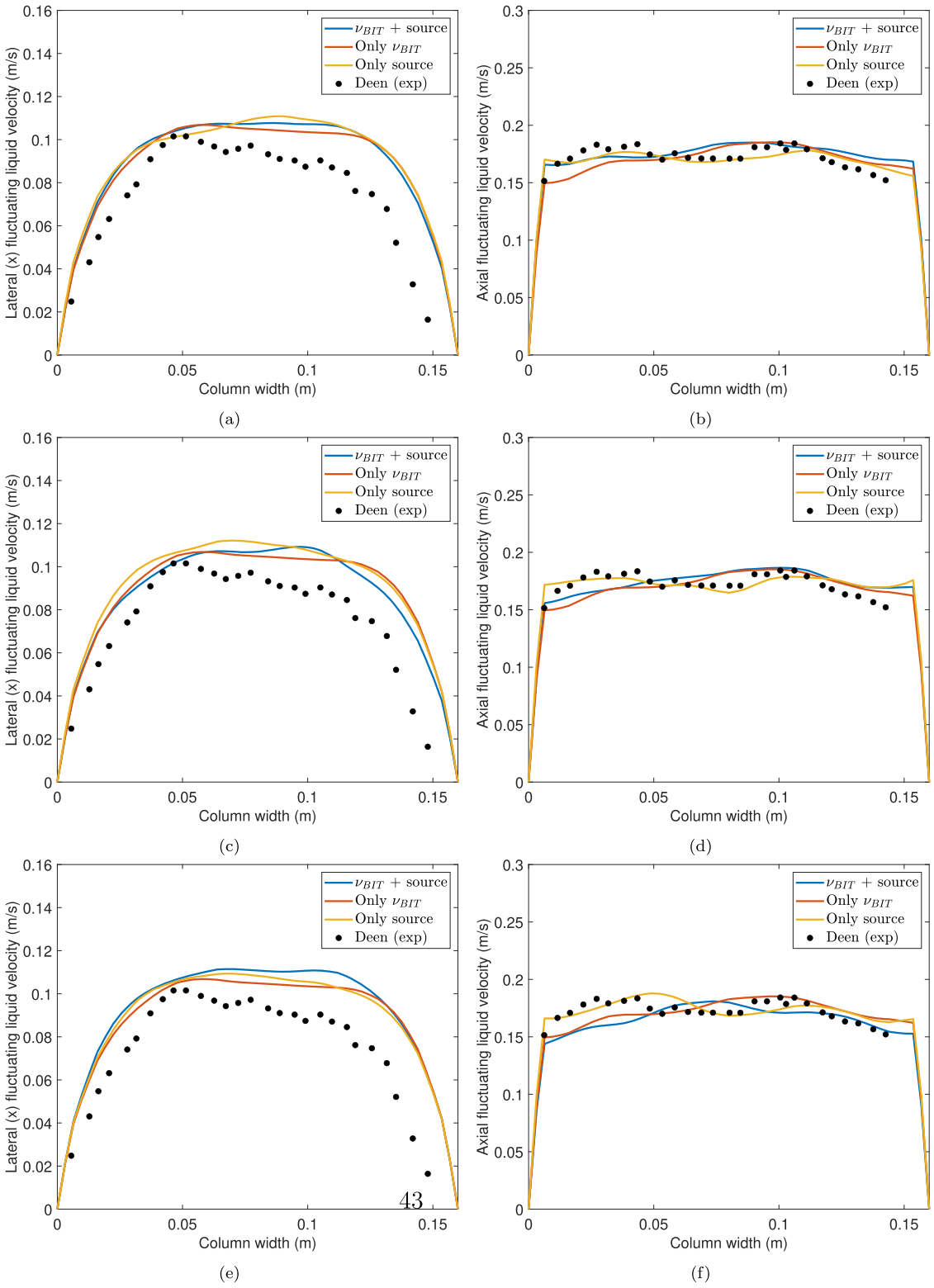

Fig. 9. Root mean square fluctuating liquid velocity using: BTS in ϵ_{SGS} source term (top), MTS in ϵ_{SGS} source term (middle), and TTS in ϵ_{SGS} source term (bottom).

work is also capable of capturing the instantaneous characteristics of the flow.

3.3. Bubble-induced turbulence modeling

In this section, the mean velocity profile of both phases, axial and lateral (transversal) fluctuating liquid velocity, and resolved turbulent kinetic energy of the liquid phase are compared with experimental data, for all cases presented in Table 2, using the finer grid, to evaluate and compare different characteristic scales of the BIT. Lastly, the comparison of instantaneous and mean values of k_{SGS} and ϵ_{SGS}, evaluated at the central point of 0.25 m measurement line is also presented.

In Fig. 8(a), the mean axial gas velocity profile using the bubble time scale shows good agreement with the experimental values, even in the

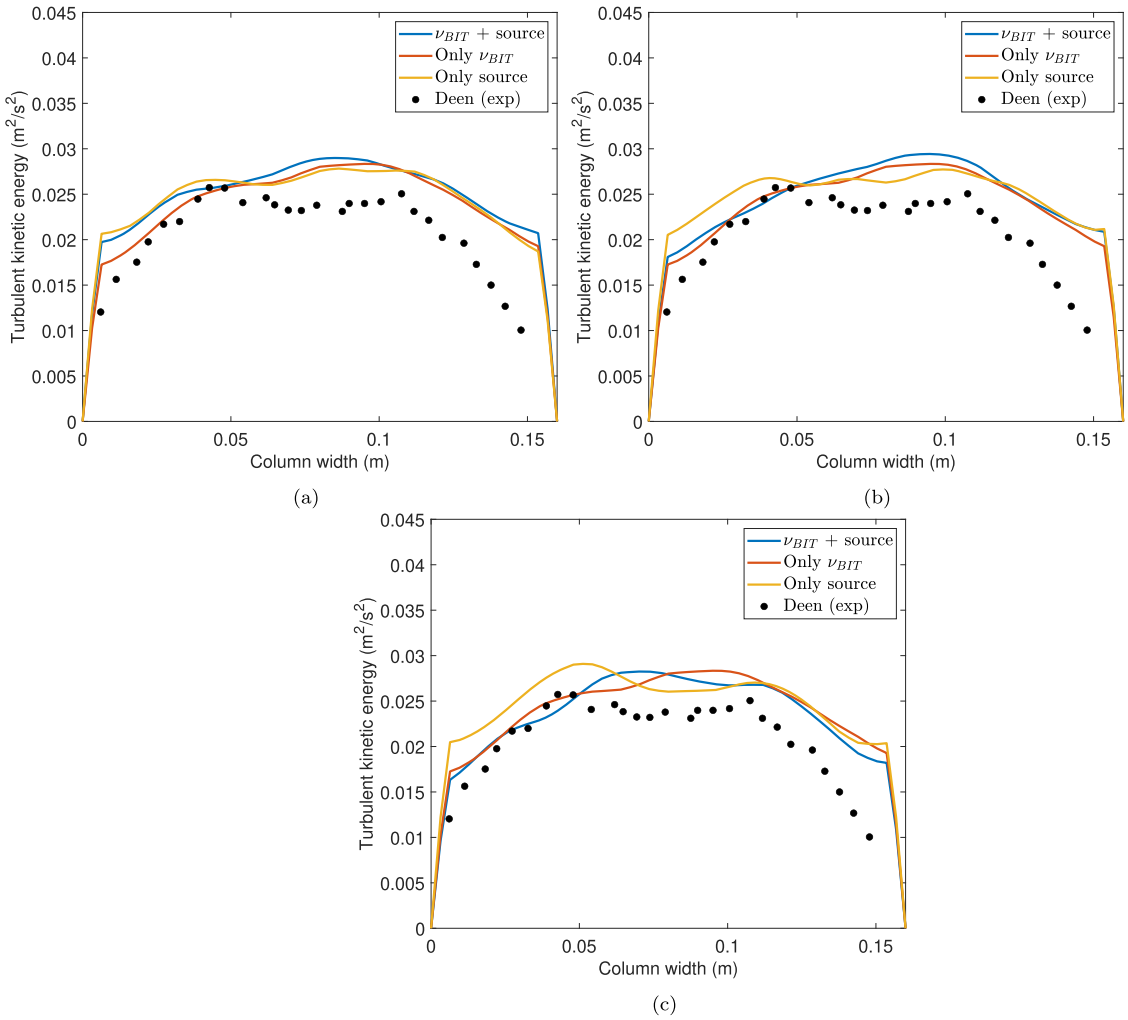

Fig. 10. Resolved turbulent kinetic energy using: (a) BTS in ε_{SGS} source term, (b): MTS in ε_{SGS} source term, and (c): TTS in ε_{SGS} source term.

near wall region, and a symmetric profile shape for all cases. A slight overestimation is observed in the center of the reactor column and may be attributed to improper estimation of the drag coefficient as observed and explained by Dhotre et al. 2008 Dhotre et al. (2008). The work of the dag force is considered the main source of BIT turbulent kinetic energy on the subgrid-scale, and other drag coefficients based on the calculated SGS energy dissipation, ε_{SGS}, such as Brucato et al. (1998) should be the subject of further investigation. The closest profile, in terms of maximum velocity, is observed for the case with ν_{BIT} and the source term in ε_{SGS}, and the most overestimated values are encountered in the case with only the source term in ε_{SGS}. With the liquid velocity, 8(b), instead, the case with only the source term in ε_{SGS} gives a better approximation of the radial distribution profile, while the case with ν_{BIT} and the source term in ε_{SGS} our model underestimates the experimental values of the axial liquid velocity. This may be attributed to an increase in the eddy viscosity in the liquid turbulence. In all cases, it is seen that it maintains the relative velocity between both phases. In addition, we analyze the effect of the other time scales in the source term ε_{SGS}. All results are consistent with those obtained with the BST source term. It can be seen from Figs. 8(c) and (d) that with the mixture time scale the case with only the source term in ε_{SGS} for bubble-induced turbulence shows better agreement with the experimental data, instead, the mean axial liquid velocity profile is underestimated compared to the experimental data. The mean axial velocities of the gas and liquid phases, using the turbulent time scale in the source term ε_{SGS} are shown in Figs. 8(e) and (e). The closest mean gas velocity to the experimental data is the case with the only source term in ε_{SGS}. It is important to mention that this model shows an improvement in both the prediction of the gas and liquid velocity.

Fig. 9 shows the root mean square of the fluctuating liquid velocity profile. For all test cases, good agreement is found for the axial fluctuating liquid velocity with all models, but not as good for the lateral component in the center region, and displays a nearly parabolic profile. This is probably due to the estimation of the mean bubble size distribution, and at the core center large bubbles move in a spiral way, as we have seen in Figure 5. The case with only the source term in ε_{SGS} gives strikingly good agreement for all tests throughout the entire column, captures the behavior of the entire profile, and reproduces the double peaks of the experimental data.

In Fig. 10, the resolved turbulent kinetic energy profiles for all cases show a good approximation of the experimental results, even in the near-wall region. However, all simulation profiles do not show the lower values encountered in the center of the column; this is probably due to the difference in the lateral fluctuating velocity profile shown in Fig. 9 and the improper interfacial forces employed, which should be further investigated. The case with only ν_{BIT} has proved to be the closest to the experimental data and the one-equation model again, at least on the left half-side of the column.

In Fig. 11, the results of instantaneous and mean values of SGS turbulent quantities at the central point of 0.25 m measurement line. The results show that ε_{SGS} greater in terms of order of magnitude than k_{SGS}. This indicates the effects of the source terms considered as closures in

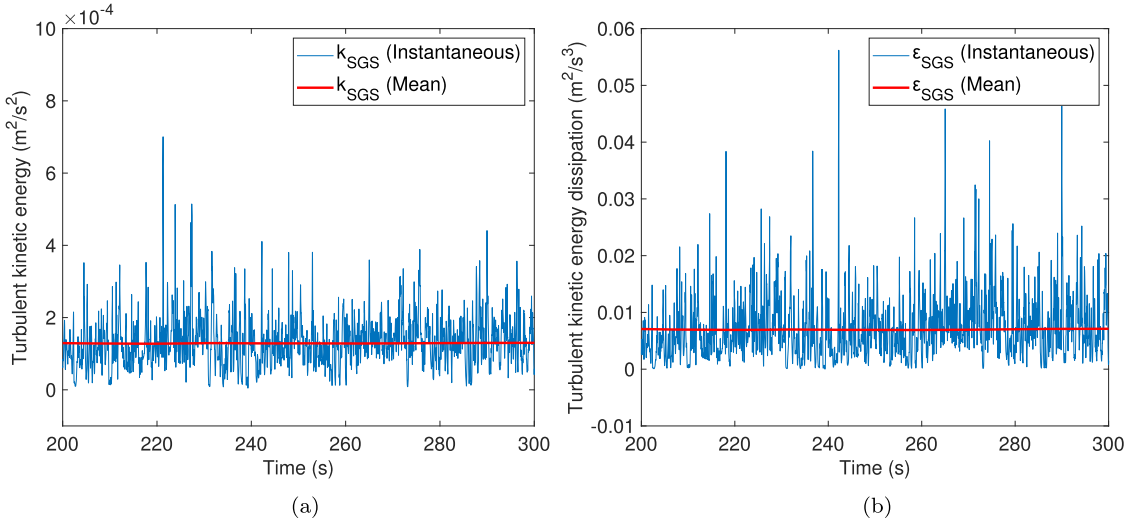

Fig. 11. Time series of instantaneous and mean sub-grid scale turbulent quantities.

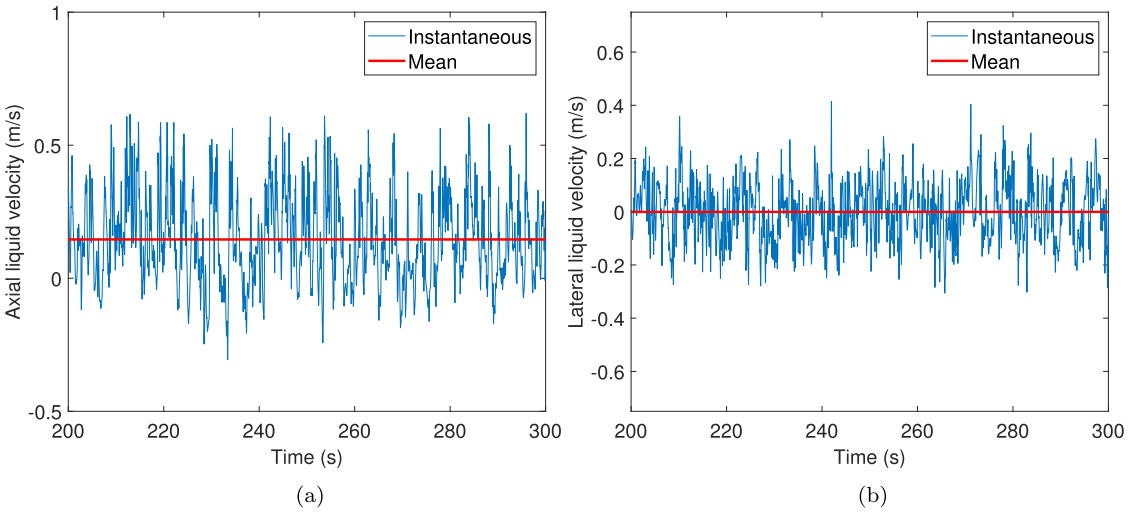

Fig. 12. Time series of instantaneous and mean liquid velocity between 200 and 300 seconds.

the two-equation LES turbulence model need to be calculated through the conservation equations (18) and (19).

3.4. Energy spectra

In Fig. 12, instantaneous axial and lateral liquid velocity time series between 200 and 300 s, with a time step of 0.001 s, and mean values are shown, which correspond to 100,000 sample values. Data are taken at the point $x = y = z = 0.25$ m. For the high frequency of data considered, the deviation of the instantaneous values around the mean with a wide range of amplitudes confirms the characteristic transient behavior of the flow and the presence of different scales.

Power spectral densities (PSD) are calculated with the data shown in Fig. 12, and a mean PSD is calculated using 20 windows of 5000 values. Pope's spectrum Pope (2001) for single-phase flow is also shown for comparison:

$$PSD(\kappa) = C\varepsilon^{2/3}\kappa^{-5/3} f_L(\kappa) f_\eta(\kappa) \tag{24}$$

$$f_L(\kappa) = \left(\frac{\kappa L}{\left[(\kappa L)^2 + C_L\right]^{1/2}} \right)^{5/3+p_0} \tag{25}$$

$$f_\eta(\kappa) = \exp\left\{ -\beta \left\{ \left[(\kappa\eta)^4 + C_\eta^4\right]^{1/4} - C_\eta \right\} \right\} \tag{26}$$

where f_L and f_η are non-dimensional functions, and L and η corresponds to the integral and Kolmogorov scales, respectively. The rest are model parameters where $C = 0.49$, $p_0 = 0$, $C_L = 6.78$, $\beta = 5.2$, and $C_\eta = 0.4$. For each velocity component, the power spectral density, shown in Fig. 13, displays a wide range of frequencies. Two characteristic regions can be observed in the inertial subrange, one with an energy decay with a slope nearly to -5/3, attributed to the shear induced turbulence by the liquid phase until approximately $\kappa_B = 1/d_B = 250$ m^{-1} (corresponding to a bubble frequency $f_B \approx 10$ Hz), meaning that the large-scale eddies are well captured, and for higher frequencies, the energy decay becomes faster with a slope around -3, as shown in the results. It is worth noting that the estimated spectrum of Pope's is in good agreement with the turbulent kinetic energy decay in both regions. Other authors analyzed the power spectral density in bubble columns using E-E with LES turbulence models and found different slope decay in the inertial subregion. For example, Dhotre et al. 2008 (Dhotre et al., 2008) found slopes of -5/3 and -10/3, Ma et al. (Ma et al., 2015) obtained a slope higher than -5/3 in the high-frequency region, while Liu et al. 2018 (Liu and Li, 2018) simulations capture the -5/3 slope in the low region frequency, but for high frequencies, they found a steeper slope of -25/3. In all cases, the faster decay in the dissipative range is attributed to the bubble-induced turbulence, and the BIT viscosity model introduced in the simulations, reinforcing the dissipative effects.

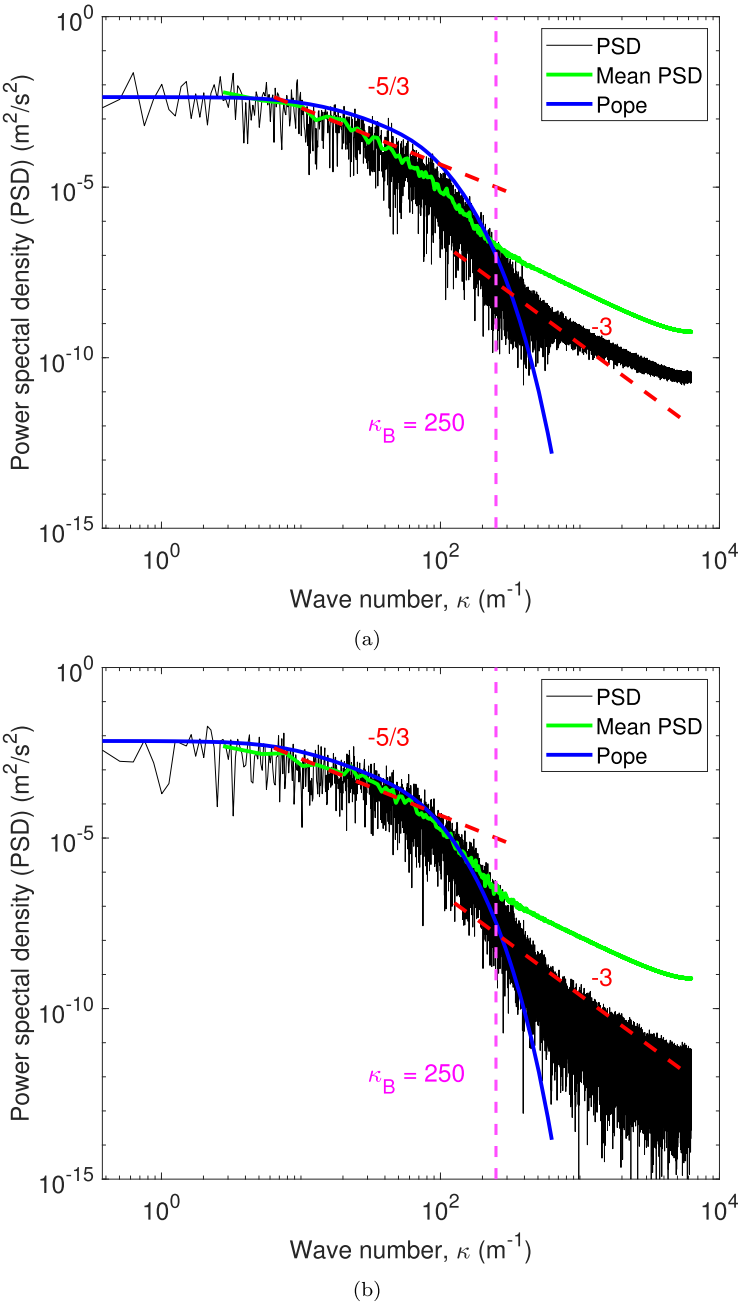

Fig. 13. Power spectral density for axial (a) and lateral (b) liquid fluctuating velocity.

The measurement values of the power spectral density in the high-frequency zone were made in (Lance and Bataille, 1991; Riboux et al., 2010; Mercado et al., 2010; Prakash et al., 2016), in which the behavior of the PSD in the inertial subrange varies from -5/3 to -3 for the lower scales in a fully turbulent flow; this change occurs at a representative bubble frequency where the dispersed phase has effects on the continuous phase. Simulations of (Long et al., 2020) and (Goraki et al., 2020a) encountered slopes of -5/3 and -3 for the PSD, and calculated the characteristic bubble frequency as $f_B = |\boldsymbol{U}_g - \boldsymbol{U}_L|/(2\pi d_B)$, obtaining approximate values of 12 and 9 Hz, respectively. Compared with other numerical studies and experimental data, it is worth noting that the results obtained in this work are consistent and within the range of expected PSD values in the low- and high-frequency regions in the inertial subrange, with a characteristic bubble frequency of 9.95 Hz, and $\boldsymbol{U}_r = |\boldsymbol{U}_g - \boldsymbol{U}_L| \approx 25$ cm/s being the bubble velocity. The decay of the power spectral density changes over this value, as shown in the present results, and the time scale $\tau = k_{SGS}/\epsilon_{SGS}$ is in the typical BIT range with a slope of -3. This suggests that this is a good estimate of the BIT time scale and that the two-fluid model has to account for the turbulent dissipation of the SGS kinetic energy.

4. Conclusion

A new two-equation subgrid-scale model for the Euler-Euler large-eddy simulation model to predict dispersed bubbly flows has been developed for gas-liquid simulation in bubble column reactors. The model was implemented in the open source OpenFOAM-v2112 code. The primary motivation to develop this model is to overcome the modeling step of the subgrid-scale turbulent dissipation rate, so that the local turbulence level can be estimated accurately which avoids calculating the SGS turbulent length without referring to mesh size. The calculated dissipation energy offers the possibility of employing various models for the

bubble-induced turbulence at the SGS level, such as those increasing the eddy viscosity or adding an extra production term to the transport equations of the SGS turbulent kinetic energy and dissipation rate. Overall, the obtained numerical results agree well with the experimental data of Deen et al. 2000, in terms of the time-averaged axial gas and liquid velocities and the resolved turbulence kinetic energy. The BIT employing the turbulent time scale either in the SGS dissipation transport equation as a source term or by the algebraic model from Sato and Sekoguchi (1975) shows the best qualitative predictions. The obtained power spectral densities show two characteristics regions that can be observed in the inertial subrange, one with an energy decay with a slope nearly to -5/3 until approximately 10 Hz, and for higher frequencies, the energy decays faster with a slope around -3. The present model requires more analysis and simulations, especially for the drag coefficient laws Brucato et al. (1998) and the mass transfer coefficient Lamont and Scott (1970) which needs accurate estimation of the SGS dissipation rate at high gas flow rates and in large bubble column reactors. Coupling the proposed model with the population balance model for accurate prediction of the bubble size distribution transfer in the pilot-scale bubble column reactor, of Gourich et al. (2005) Gourich et al. (2006) and Kouzbour et al. (2021) Kouzbour et al. (2021) at higher inlet superficial gas velocities and where accurate prediction of SGS turbulent dissipation rate from a transport equation is an important input parameter for closure models of coalescence and break-up, is under way and will be reported in a future work.

CRediT authorship contribution statement

Diego González: Writing – review & editing, Visualization, Validation, Software, Methodology, Investigation, Conceptualization; **Anton Vernet:** Writing – review & editing; **Bouchaib Gourich:** Writing – review & editing, Investigation; **Youssef Stiriba:** Writing – review & editing, Visualization, Supervision, Software, Methodology, Investigation, Conceptualization.

Data availability

Data will be made available on request.

Declaration of competing interest

The authors declare that they have no known competing financial interests or personal relationships that could have appeared to influence the work reported in this paper.

References

Auton, T.R., 1987. The lift force on a spherical body in a rotational flow. J. Fluid Mech. 183, 199–218.

Behzadi, A., Issa, R.I., Rusche, H., 2004. Modelling of dispersed bubble and droplet flow at high phase fractions. Chem. Eng. Sci. 59 (4), 759–770.

Lopez de Bertodano, M., Lahey, R.T., Jones, O.C., 1994. Development of a k-ε model for bubbly two-phase flow. J. Fluids Eng. 116 (1), 128–134.

Brucato, A., Grisafi, F., Montante, G., 1998. Particle drag coefficients in turbulent fluids. Chem. Eng. Sci. 53 (18), 3295–3314.

Chaouat, B., Schiestel, R., 2005. A new partially integrated transport model for subgrid-scale stresses and dissipation rate for turbulent developing flows. Phys. Fluids 17 (6).

Chen, R.C., Reese, J., Fan, L.-S., 1994. Flow structure in a three-dimensional bubble column and three-phase fluidized bed. AlChE J. 40 (7), 1093–1104.

Clift, R., Grace, J.R., Weber, M.E., 1978. Bubbles, drops, and particles. Academic Press, New York, USA.

Deen, N.G., Solberg, T., Hjertager, B.H., 2001. Large eddy simulation of the gas–liquid flow in a square cross-sectioned bubble column. Chem. Eng. Sci. 56 (21–22), 6341–6349.

Degaleesan, S., Dudukovic, M., Pan, Y., 2001. Experimental study of gas-induced liquid-flow structures in bubble columns. AlChE J. 47 (9), 1913–1931.

Dhotre, M.T., Deen, N.G., Niceno, B., Khan, Z., Joshi, J.B., 2013. Large eddy simulation for dispersed bubbly flows: a review. Int. J. Chem. Eng. 2013 (1), 343276.

Dhotre, M.T., Niceno, B., Smith, B.L., 2008. Large eddy simulation of a bubble column using dynamic sub-grid scale model. Chem. Eng. J. 136 (2–3), 337–348.

Drew, D.A., Lahey, J.R.T., 1987. The virtual mass and lift force on a sphere in rotating and straining inviscid flow. Int. J. Multiphase Flow 13 (1), 113–121.

Germano, M., Piomelli, U., Moin, P., Cabot, W.M., 1991. A dynamic subgrid-scale eddy viscosity model. Phys. Fluids A: Fluid Dyn. 3 (7), 1760–1765.

Goraki, M.G.F., Stiriba, Y., Gourich, B., Vial, C., Grau, F.X., 2020a. Euler-euler large eddy simulations of the gas–liquid flow in a cylindrical bubble column. Nucl. Eng. Des. 369, 110823.

Goraki, M.G.F., Vernet, A., Stiriba, Y., Grau, X., 2020b. Transient large-scale two-phase flow structures in a 3d bubble column reactor. Int. J. Multiphase Flows 127, 103236.

Gourich, B., Vial, C., Essadki, A.H., Allam, F., Soulami, M.B., Ziyad, M., 2006. Identification of flow regimes and transition points in a bubble column through analysis of differential pressure signal?influence of the coalescence behavior of the liquid phase. Chem. Eng. Process. 45 (3), 214–223.

Han, L., M. Li, J.F., Gong, S., Gao, N., Zhang, C., Luo, H., 2016. A theoretical unsteady-state model for k_l of bubbles based on the framework of wide energy spectrum. AlChE J. 62 (4), 1007–1022.

Ishii, M., Zuber, N., 1979. Drag coefficient and relative velocity in bubbly, droplet or particulate flows. AlChE J. 25 (5), 843–855.

Joshi, J.B., 2001. Computational flow modelling and design of bubble column reactors. Chem. Eng. Sci. 56 (21–22), 5893–5933.

Kataoka, I., Serizawa, A., Besnard, D.C., 1993. Prediction of turbulence suppression and turbulence modeling in bubbly two-phase flow. Nucl. Eng. Des. 141 (1–2), 145–158.

Kouzbour, S., Gourich, B., Cockx, A., Stiriba, Y., 2025. Development and validation of 1d gas-liquid model for dissolved mn(II) removal by oxidation process in a square bubble column. Chem. Eng. Sci. 302, 120815.

Kouzbour, S., Gourich, B., Stiriba, Y., Vial, C., Gros, F., Sotudeh-Gharebagh, R., 2021. Experimental analysis of the effects of liquid phase surface tension on the hydrodynamics and mass transfer in a square bubble column. Int. J. Heat Mass Transf. 170, 121009.

Lakehal, D., 2018. Status and future developments of large-eddy simulation of turbulent multi-fluid flows (LEIS and LESS). Int. J. Multiphase Flow 104, 322–337.

Lamont, J.C., Scott, D.S., 1970. An eddy cell model of mass transfer into the surface of a turbulent liquid. AlChE J. 16 (4), 513–519.

Lance, M., Bataille, J., 1991. Turbulence in the liquid phase of a uniform bubbly air–water flow. J. Fluid Mech. 222, 95–118.

Liao, Y., Ma, T., Krepper, E., Lucas, D., Fröhlich, J., 2019. Application of a novel model for bubble-induced turbulence to bubbly flows in containers and vertical pipes. Chem. Eng. Sci. 202, 55–69.

Liu, Z., Li, B., 2018. Scale-adaptive analysis of euler-euler large eddy simulation for laboratory scale dispersed bubbly flows. Chem. Eng. J. 338, 465–477.

Liu, Z., Wu, Y., Li, B., 2020. An assessment of the peformance of sub-gbrid scale models of large-eddy simulation in modeling bubbly flows. Powder Technol. 374, 470–481.

Long, S., Yang, J., Huang, X., Li, G., Shi, W., Sommerfeld, M., Yang, X., 2020. Large-eddy simulation of gas–liquid two-phase flow in a bubble column reactor using a modified sub-grid scale model with the consideration of bubble-eddy interaction. Int. J. Heat Mass Transf. 161, 120240.

Ma, T., Ziegenhein, T., Lucas, D., Krepper, E., Fröhlich, J., 2015. Euler–euler large eddy simulations for dispersed turbulent bubbly flows. Int. J. Heat Fluid Flow 56, 51–59.

Ma, T., Ziegenhein, T., Lucas, D., Krepper, E., Fröhlich, J., 2016. Large eddy simulations of the gas–liquid flow in a rectangular bubble column. Nucl. Eng. Des. 299, 146–153.

Masood, R.M.A., Delgado, A., 2014. Numerical investigation of the interphase forces and turbulence closure in 3d square bubble columns. Chem. Eng. Sci. 108, 154–168.

Mercado, J.M., Gomez, D.C., van Gils, D., Sun, C., Lohse, D., 2010. On bubble clustering and energy spectra in pseudo-turbulence. J. Fluid Mech. 650, 287–306.

Milelli, M., 2002. A numerical analysis of confined turbulent bubble plumes. Ph.D. thesis. ETH Zurich.

Mudde, R.F., Simonin, O., 1999. Two-and three-dimensional simulations of a bubble plume using a two-fluid model. Chem. Eng. Sci. 54 (21), 5061–5069.

Ničeno, B., Dhotre, M.T., Deen, N.G., 2008. One-equation sub-grid scale (SGS) modelling for euler–euler large eddy simulation (EELES) of dispersed bubbly flow. Chem. Eng. Sci. 63 (15), 3923–3931.

Perot, J.B., Gadebusch, J., 2007. A self-adapting turbulence model for flow simulation at any mesh resolution. Phys. Fluids 19 (11), 115105.

Pfleger, D., Becker, S., 2001. Modelling and simulation of the dynamic flow behaviour in a bubble column. Chem. Eng. Sci. 56 (4), 1737–1747.

Pfleger, D., Gomes, S., Gilbert, N., Wagner, H.-G., 1999. Hydrodynamic simulations of laboratory scale bubble columns fundamental studies of the eulerian–eulerian modelling approach. Chem. Eng. Sci. 54 (21), 5091–5099.

Pope, S.B., 2001. Turbulent Flow. Cambridge University Press, Cambridge, UK.

Prakash, V.N., Mercado, J.M., van Wijngaarden, L., Mancilla, E., Tagawa, Y., Lohse, D., Sun, C., 2016. Energy spectra in turbulent bubbly flows. J. Fluid Mech. 791, 174–190.

Riboux, G., Risso, F., Legendre, D., 2010. Experimental characterization of the agitation generated by bubbles rising at high reynolds number. J. Fluid Mech. 643, 509–539.

Rusche, H., 2002. Computational fluid dynamics of dispersed two-phase flows at high speed fractions. Ph.D. thesis. PhD thesis, Imperial College of Science, Technology and Medicine.

Rzehak, R., Krepper, E., 2013a. Bubble-induced turbulence: comparison of CFD models. Nucl. Eng. Des. 258, 57–65.

Rzehak, R., Krepper, E., 2013b. CFD Modeling of bubble-induced turbulence. Int. J. Multiphase Flow 55, 138–155.

Sato, Y., Sekoguchi, K., 1975. Liquid velocity distribution in two-phase bubble flow. Int. J. Multiphase Flow 2 (1), 79–95.

Simonnet, M., Gentric, C., Olmos, E., Midoux, N., 2007. Experimental determination of the drag coefficient in a swarm of bubbles. Chem. Eng. Sci. 62 (3), 858–866.

Tabib, M.V., Roy, S.A., Joshi, J.B., 2008. CFD Simulation of bubble column-an analysis of interphase forces and turbulence models. Chem. Eng. J. 139 (3), 589–614.

Tomiyama, A., Tamai, H., Zun, I., Hosokawa, S., 2002. Transverse migration of single bubbles in simple shear flows. Chem. Eng. Sci. 57 (11), 1849–1858.

Troshko, A.A., Hassan, Y.A., 2001. A two-equation turbulence model of turbulent bubbly flows. Int. J. Multiphase Flow 27 (11), 1965–2000.
Vial, C., Stiriba, Y., 2013. Characterization of bioreactors using computational fluid dynamics. In: Fermentation Processes Engineering in the Food Industry. Taylor & Francis Group, pp. 121–164.
Wang, G., Yang, F., Wu, K., Ma, Y., Peng, C., Liu, T., Wang, L.-P., 2021. Estimation of the dissipation rate of turbulent kinetic energy: a review. Chem. Eng. Sci. 229, 116133.
Weller, H.G., OpenCFD, Ltd., 2005. Derivation, Modelling and Solution of the Conditionally Averaged Two-Phase Flow Equations.
Weller, H.G., Tabor, G., Jasak, H., Fureby, C., 1998. A tensorial approach to computational continuum mechanics using object-oriented techniques. Comput. Phys. 12 (6), 620–631.
Zhang, D., Deen, N.G., Kuipers, J.A.M., 2006. Numerical simulation of the dynamic flow behavior in a bubble column: a study of closures for turbulence and interface forces. Chem. Eng. Sci. 61 (23), 7593–7608.